J. Fluid Mech. (2019), *vol.* 865, R1, doi:10.1017/jfm.2019.131

JFM RAPIDS
journals.cambridge.org/rapids

The meandering behaviour of large-scale structures in turbulent boundary layers

Kevin[1,†], Jason Monty[1] and Nicholas Hutchins[1]

[1]Department of Mechanical Engineering, University of Melbourne, Victoria 3010, Australia

(Received 26 November 2018; revised 24 January 2019; accepted 10 February 2019;
first published online 27 February 2019)

This paper quantifies the instantaneous form of large-scale turbulent structures in canonical smooth-wall boundary layers, demonstrating that they adhere to a form that is consistent with the self-sustaining streak instability model suggested by Flores & Jiménez (*Phys. Fluids*, vol. 22, 2010, 071704) and Hwang & Cossu (*Phys. Fluids*, vol. 23, 2011, 061702). Our motivation for this study stems from previous observations of large-scale streaks that have been spatially locked in position within spanwise-heterogeneous boundary layers. Here, using similar tools, we demonstrate that the randomly occurring large-scale structures in canonical layers show similar behaviour. Statistically, we show that the signature of large-scale coherent structures exhibits increasing meandering behaviour with distance from the wall. At the upper edge of the boundary layer, where these structures are severely misaligned from the main-flow direction, the induced velocities associated with the strongly yawed vortex packets/clusters yield a significant spanwise-velocity component leading to an apparent oblique coherence of spanwise-velocity fluctuations. This pronounced meandering behaviour also gives rise to a dominant streamwise periodicity at a wavelength of approximately 6δ. We further statistically show that the quasi-streamwise roll-modes formed adjacent to these very large wavy motions are often one-sided (spanwise asymmetric), in stark contrast to the counter-rotating form suggested by conventional conditionally averaged representations. To summarise, we sketch a representative picture of the typical large-scale structures based on the evidence gathered in this study.

Key words: boundary layer structure, turbulent boundary layers

1. Introduction

Portraying instantaneous wall turbulence using its representative structure is useful for modelling and for the development of our understanding. However, as expressed by Jiménez (2018), this implementation 'should be undertaken with proper care to distinguish between what is important for the system and what is convenient for

† Email address for correspondence: kevin.kevin@unimelb.edu.au

us'. There are often questions regarding how well the average coherence resembles the instantaneous structures. An example here could be the notional representation of large-scale low-momentum structures as streamwise aligned and symmetrically flanked by two high-speed regions, e.g. figure 18 of Dennis & Nickels (2011), or figure 9 of Hutchins *et al.* (2012). An obvious question here is whether this largely symmetrical coherence is truly a dominant feature in the instantaneous flow, or if it appears due to averaging procedures applied in spanwise-homogeneous flow fields.

With care, deeper elucidation can be obtained by adding certain conditions to the averaging process. For instance, Johansson, Alfredsson & Kim (1991) preserved the non-symmetrical nature of buffer-region structures by adding a spanwise-velocity criterion to the detection. They concluded that asymmetric structures occur more often than the symmetric ones, and this asymmetry is important for the evolution of shear layers. At a much larger scale, the meandering behaviour of the log-region structures (Hutchins & Marusic 2007; Monty *et al.* 2007) highlights the asymmetric nature of large-scale turbulence. Accordingly, it was suggested that the weak 'X'-shape pattern which manifests in the average coherence, when viewed in the horizontal plane, is indicative of a combination of individual events that are tilted in either the positive or negative spanwise direction. A subsequent investigation using a multi-point detection technique (targeting spanwise asymmetry in $\mathrm{d}u_\tau/\mathrm{d}x$ about the condition point) by Hutchins *et al.* (2011) gave an initial quantification of how often this meandering behaviour occurs. The present analysis further dissects this behaviour from a different perspective.

To an extent, the difficulty in elucidating the behaviour of turbulence structures is due to their random occurrence in space and time. In fact, when a dominant structure can be isolated and scrutinised, as is the case in a 'minimal' numerical domain (Jiménez & Simens 2001; Flores & Jiménez 2010), its important dynamical properties can be unravelled.

In a similar vein, we have been able to scrutinise the large-scale streaks in heterogeneous boundary layers (Kevin *et al.* 2017; Kevin, Monty & Hutchins 2019) owing to the spatial locking of these features at certain phases of the spanwise heterogeneity. In these previous experiments, the spanwise heterogeneity was imposed by a herringbone riblet surface, which generates locked low-speed streaks over the converging region and high-momentum streaks over the diverging region of the surface texture. In that case, we observed that the instantaneous large-scale streamwise vortices which border the low-momentum regions are intermittent in time and space, with one-sided asymmetric flanking vortices occurring more often that the two-sided/counter-rotating features that are often inferred from time averaging. Additionally, it was observed that the streaks in the outer layer exhibit a strong meandering behaviour. In the cross-stream plane, this behaviour corresponds to a vertical tilting/leaning of the taller ejection events in the spanwise direction. This apparent meandering behaviour imparts a strong streamwise periodicity on the spatial statistics that can be readily discerned in the instantaneous flow fields at certain locations within the spanwise-heterogeneous layer. It will be shown here that similar behaviours are also present in the naturally occurring large-scale features that populate canonical (spanwise-homogeneous) turbulent boundary layers, though they occur randomly in time and space.

1.1. *Inspirations and aims of the present study*

Other behaviours of the low-momentum regions observed in spanwise-heterogeneous flows, such as over heterogeneous surfaces (e.g. Vanderwel & Ganapathisubramani

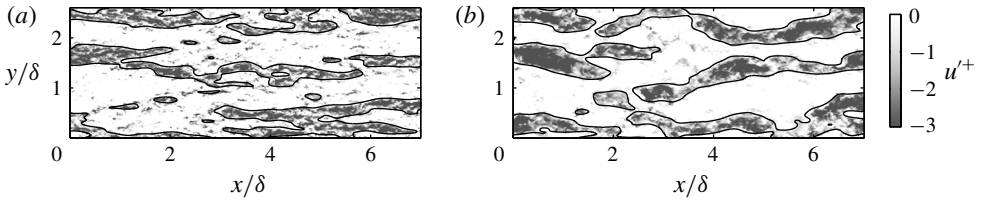

FIGURE 1. An example of wall-parallel (top-view) signature of streamwise-velocity fluctuations (a) in the log region at $z/\delta = 0.07$, showing contours of $u' = -0.7U_\tau$, and (b) in the outer layer at $z/\delta = 0.4$, showing $u' = -0.5U_\tau$. Taken from an instantaneous volumetric DNS dataset of Sillero, Jiménez & Moser (2014). Note that here y-axis represents the spanwise direction.

2015; Bai *et al.* 2018; Kevin *et al.* 2019, among others) and in boundary layers evolving downstream of vortex generators (Baidya *et al.* 2016), differ from the structures that naturally form in smooth-wall layers, principally because the spanwise wavelength is mechanically prescribed by the perturbation. However, we also notice many surprising similarities between the artificially stimulated and the naturally developed large-scale motions. The streaky log-region coherence in smooth-wall (spanwise-homogeneous) boundary layers, as shown in figure 1(a), has been well studied (e.g. by Tomkins & Adrian 2003; Lee *et al.* 2014). The outer-layer signature of the same instance, however, as shown by figure 1(b), displays a less familiar behaviour, namely a more pronounced undulating/meandering appearance (later quantified in § 2). Interestingly, this behaviour mimics that of the artificially generated streaks studied by Kevin *et al.* (2019) in spanwise-heterogeneous boundary layers. Thus far, this outer asymmetric meandering behaviour has received scant attention, and largely remains absent from certain models of large-scale coherent motions (e.g. Adrian, Meinhart & Tomkins 2000*b*; Marusic & Monty 2019).

By employing the boundary layer DNS database of Sillero *et al.* (2014) at $Re_\tau \approx 2000$ and experimental datasets of de Silva *et al.* (2018) and Kevin *et al.* (2019) at similar Reynolds numbers, here we aim to elucidate the large-scale motions in canonical boundary layers using statistical techniques that were developed by Kevin *et al.* (2017, 2019) for the study of spanwise-heterogeneous flows. The collective understanding developed here further provides insight into other boundary layer phenomena, such as the oblique patterns in spanwise-velocity coherence (Sillero *et al.* 2014; de Silva *et al.* 2018). Finally, we offer a schematic representation of the large-scale turbulence arrangement based on the insight gained from this study.

2. An increasingly meandering signature with distance from the wall

Throughout this paper x, y and z refer to the streamwise, spanwise and wall-normal directions, with u, v and w indicating the respective total velocity components.

We first quantify how the large low-momentum regions become increasingly wavy with distance from the wall. In figure 2(a), the grey-shaded regions indicate the filtered signature of $u'_f < 0$ (subscript f denotes filtered quantity) for the example shown in figure 1(b). For this wall height ($z/\delta = 0.4$), we apply a 2D Gaussian filter ($\sigma = 2$) with the size of $2.1 \times 0.43\delta$ in the $x \times y$ direction. This filter size corresponds to the length and width of the correlation function $R_{u'u'} = 0.15$, hence it is a function of wall height. Note that the change in $R_{u'u'}$ dimension (i.e. our filter size) with wall height is

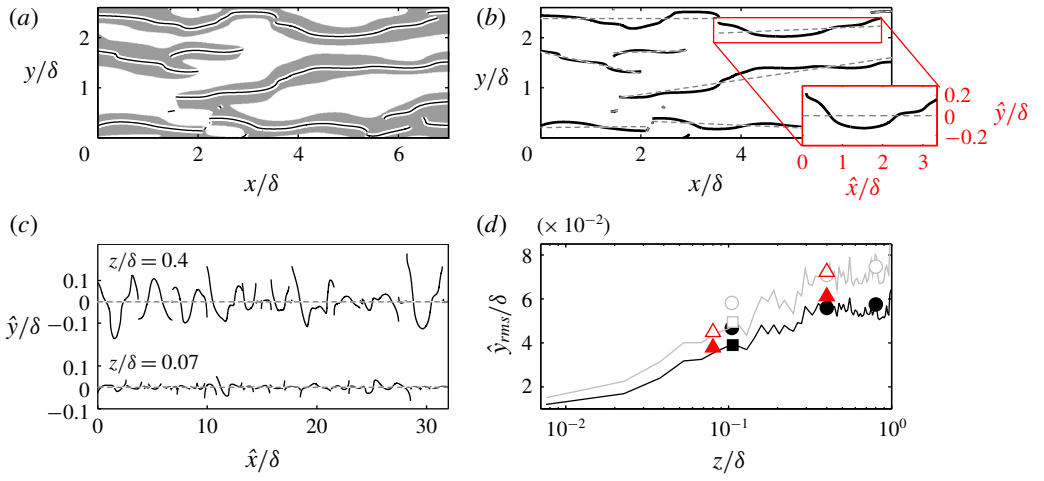

FIGURE 2. (*a*) Grey regions: $u_f' < 0$ at $z/\delta = 0.4$, highlighting the spine of each region. (*b*) Dotted line: the linear fit of each spine. Inset shows $\hat{x}$, the projected linear fit to the streamwise direction; $\hat{y}$: the projected spine about the linear fit. (*c*) The concatenation of the spines about their individual fitted line. (*d*) The meandering root mean square as a function of wall height. Lines: dataset of Sillero *et al.* (2014); squares: smooth-wall data of Kevin *et al.* (2019); circles: de Silva *et al.* (2018). Black line and closed symbols: cases where spines are longer than the filter size. Grey line and open symbols: cases where spines are longer than twice the filter size. Triangles: artificially generated streaks over herringbone riblets (Kevin *et al.* 2019).

well documented in the literature (Tomkins & Adrian 2003; Ganapathisubramani *et al.* 2005; Lee & Sung 2011; Sillero *et al.* 2014). From this filtered field, we can identify the 'spine' of each low-momentum region by finding the local minima of $\partial u/\partial y = 0$ at every streamwise position, in a similar approach to that followed by Schoppa & Hussain (2002). To gauge the meandering behaviour, we quantify the 'waviness' of these spines and employ it as a metric. In this manner, the width of the structure does not play any role in the quantification. In figure 2(*b*), the dashed line plotted over each spine indicates its linear fit. Accordingly, we treat these spines as fluctuation signals $\hat{y}$ about the fitted line (see inset). This also means that the linear orientation of the spines will not be considered. The concatenated 'spine signals' are displayed in figure 2(*c*), where we compare the projected signals for $z/\delta = 0.07$ and 0.4.

We can now compute the root mean square of these signals for multiple wall heights, and the trend is shown in figure 2(*d*). Note that we only consider the individual spine that is longer than the filter size, where the results are shown by the black line and closed symbols. Clearly this metric ($\hat{y}_{rms}$) indicates that the spine of low-momentum regions increasingly fluctuates with wall distance, and the trend is consistent across numerical and experimental datasets. It is noted that the meandering amplitude flattens for $z/\delta > 0.5$. This is partly because the detected structures become shorter/patchier in the turbulent-intermittent region, which will bias the meandering detection (i.e will limit $\hat{y}_{rms}$). As a check, when we consider only those spines that are longer than twice the filter size (denoted by the grey line and open symbols), the overall meandering magnitude increases and we observe less flattening away from the wall. It is important to note that here we simply aim to demonstrate statistically that

large-scale turbulence becomes increasingly wavy with wall distance, without putting emphasis on the exact rate of the increase.

Finally, the triangle symbols in figure 2(*d*) indicate the meandering magnitude of the artificially generated streaks studied by Kevin *et al.* (2019) in a spanwise-heterogeneous boundary layer (where the global or spanwise-averaged δ is used to normalise), and the results closely conform to the increasing trend of the canonical case. This observation suggests that the pronounced undulating behaviour, that in Kevin *et al.* (2019) was attributed to the imposed turbulent secondary flows, is in fact an underlying characteristic of large-scale turbulence structures.

2.1. *Severely meandering turbulent signature at the edge of the boundary layer*

Sillero *et al.* (2014) reported that the spanwise-velocity component exhibits a large oblique/diagonal coherence. The $\pm 45^\circ$ (from streamwise axis) pattern is particularly discernible in the outermost part of the boundary layer. The coherence emerges statistically (e.g. in 2D correlation), if one decomposes by either the positive or negative spanwise-velocity sign. Thus far, little physical interpretation has been given to this phenomenon. de Silva *et al.* (2018) described this occurrence as the spanwise-velocity signature of the arched head of a hairpin-type eddy. Indeed, when one considers the positive or negative spanwise velocity on a wall-parallel slice close to the head of a hairpin eddy, the imprints are diagonally positioned. Note that in making this observation, de Silva *et al.* (2018) did observe that, in reality the obliqueness may involve 'a range of representative eddies which are not necessarily forced to be streamwise aligned or symmetric'. In this spirit, we build on these previous observations of this unique oblique turbulent pattern.

Figure 3(*a*,*b*) shows an instance of streamwise and spanwise velocity at $z = \delta_{99}$ at a different instance to that shown in figures 1 and 2. This snapshot is selected since it effectively highlights the oblique v pattern as discussed by Sillero *et al.* (2014) and de Silva *et al.* (2018). When carefully examining many vector fields around similar oblique features, such as in figure 3(*c*–*e*), we observed that the low-speed (streamwise negative) fluctuations associated with vortex groups, which are typically more streamwise aligned, are now consistently oriented at approximately $\pm 45^\circ$. This is further illustrated by the compact swirling-strength contours, λ_{ci} (computed using the method described in Adrian, Christensen & Liu (2000*a*)), which indicate the presence of wall-normal vortices in figure 3(*c*–*e*). Note that in these figures they appear to be roughly aligned along the diagonals. Based on these simple observations, we surmise that the negative u' fluctuations associated with vortex packets (Adrian *et al.* 2000*b*) or clusters (del Álamo *et al.* 2006), which themselves are often yawed or appear oblique in the outer region, are resolved or decomposed in the y-direction as these oblique v features. Not only does this observation provide an extension to the work of Sillero *et al.* (2014) and de Silva *et al.* (2018) regarding the emergence of these oblique patterns in v, it also further demonstrates that turbulent events become increasingly misaligned from the main-flow direction with wall height. As a final point, the lesser degree of meandering at lower wall heights further explains why the apparent v diagonals are less oblique closer to the wall at much smaller angles than $\pm 45^\circ$. This behaviour was also observed by de Silva *et al.* (2018) in the log region, though at the time an explanation for this observation was still lacking.

3. Outer-layer periodicity of the large structures

In a spanwise-heterogeneous boundary layer (*viz.* over herringbone roughness), where the large-scale low-momentum regions were forcibly formed at fixed spanwise

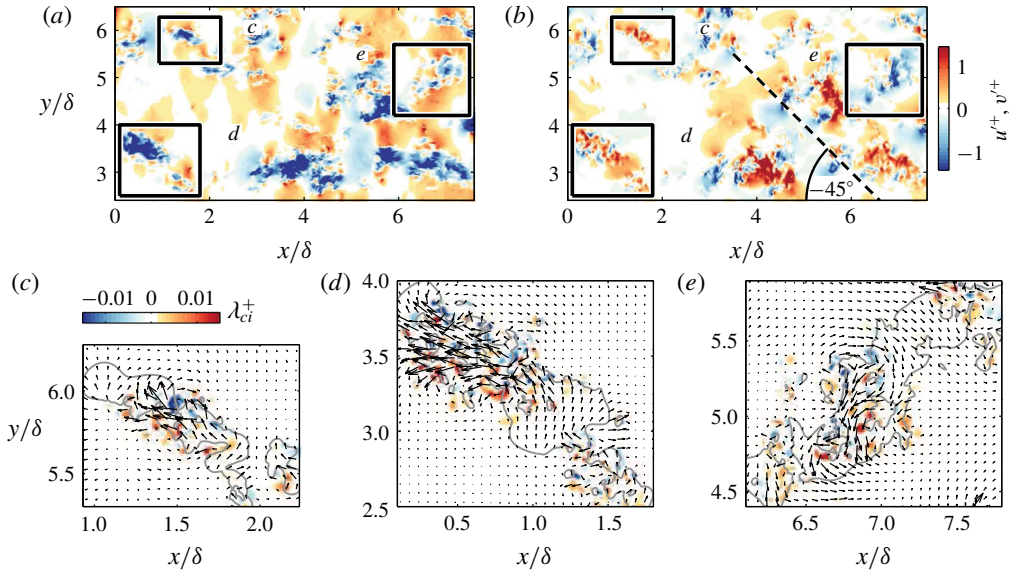

FIGURE 3. Example of (*a*) streamwise-velocity and (*b*) spanwise-velocity field at $z = \delta_{99}$, highlighting several oblique v features. Taken from dataset of Sillero *et al.* (2014). Square insets highlight particular inclined features that are magnified in the following subfigures. (*c–e*) Vectors of velocity fluctuations, with contour of signed swirling strength λ_{ci} superimposed. Grey contour lines show $v^+ = 0.3$ in (*b*,*c*) and $v^+ = -0.3$ in (*d*).

locations, Kevin *et al.* (2019) observed a dominant streamwise-repeating behaviour of those low-momentum structures. This outer-layer pattern emerged in the correlation-coefficient map, $R_{u'u'}$, when it was computed at a spanwise reference location midway between where the low- and high-momentum regions were induced. In spanwise-homogeneous (smooth-wall) boundary layers however, where these turbulent regions occur spatially and temporally at random, extracting such repeating patterns becomes less straightforward.

3.1. *Detection of low-momentum structures*

Here we aim to show that the streamwise-repeating behaviour is also prevalent in smooth-wall boundary layers. Since volumetric datasets are required in this elucidation, we extract and use $x \times y \times z = 8\delta \times 8\delta \times 1.2\delta$ domains from the boundary layer DNS data of Sillero *et al.* (2014) at the highest Reynolds number streamwise location available ($Re_\tau \approx 2000$), which is comparable to our experimental datasets. Figure 4 illustrates how we detect and isolate the large-scale structures. The low-momentum regions are first located by observing their horizontal signature in the log region, as shown in figure 4(*a*). Here the filtered streamwise-velocity fluctuations u'_f (filtered as in § 2) at $z/\delta = 0.07$ are spatially averaged in the streamwise direction over the 8δ-long extracted domain, resulting in a spanwise distribution of $\langle u'_f \rangle_x$ which is displayed in figure 4(*b*) for this instance. The low-speed signatures where $\langle u'_f \rangle_x^+ < -0.5$ approximate the spanwise locations where relatively long streaks occur. The '+' symbols in figure 4(*c*) illustrate the locations of the eight detected structures that appear in this instance. Subsequently, we can now extract narrow ($x \times y \times z = 8\delta \times 1.2\delta \times 1.2\delta$) volumetric subsets as shown in figure 4(*d*), in which

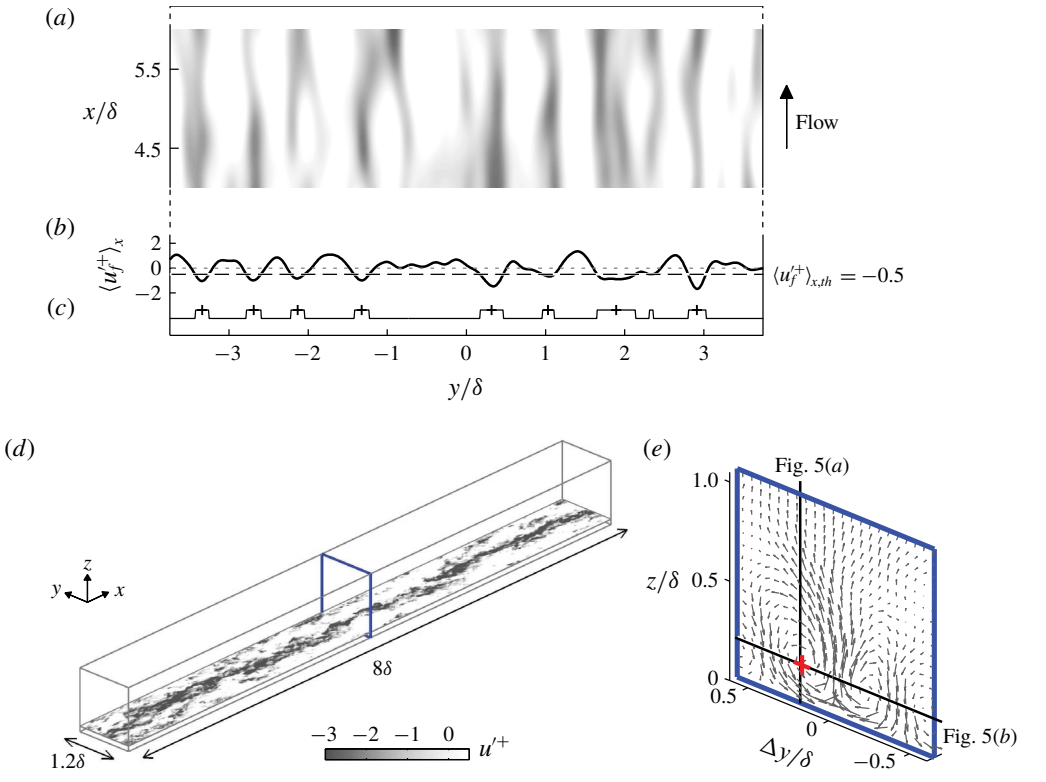

FIGURE 4. Detection of low-speed streaks from the dataset of Sillero *et al.* (2014). (*a*) A wall-parallel (top-view) snapshot, showing filtered velocity u'_f at $z/\delta = 0.07$. Only a subset of the extracted data is plotted from a total of 8δ streamwise domain. (*b*) Distribution of streamwise-averaged velocity within the entire 8δ-long domain, $\langle u'_f \rangle_x$. (*c*) A logic signal for the condition $\langle u'_f \rangle_x < -0.5$. The + symbols show the spanwise centre of the detected streaks. (*d*) An example wall-parallel slice of streamwise-velocity fluctuations at $z/\delta = 0.07$ corresponding to one of the detected streaks, showing a continuous long low-momentum region within the narrow extracted domain. (*e*) The ensemble-averaged V and W vectors on the cross-plane marked in (*d*). Here $\Delta y = 0$ indicates the centre of the extracted domain. The + (red) symbol indicates the reference point $(\Delta y_{ref}, z_{ref})/\delta = (0.2, 0.2)$ where the correlation maps shown later in figure 5 are computed, and the black lines illustrates the corresponding vertical and horizontal planes.

the low-momentum regions on average occur at the spanwise centre of this volume. A total of 50 such streaks are identified from eight DNS fields used in the present analysis, and the ensemble-averaged motions on a cross-stream plane are shown in figure 4(*e*).

3.2. *Spatial statistics in the outer layer*

As a conjecture, we associate the collection of streaks in smooth-wall boundary layers (identified above) and the accompanying roll-modes shown in figure 4(*e*), to the continuous low-momentum regions that occur in spanwise-heterogeneous layers and the associated 'mean secondary flows/roll-modes'. Hence, we will replicate the analysis of Kevin *et al.* (2019) for spanwise-heterogeneous layers, in order to extract

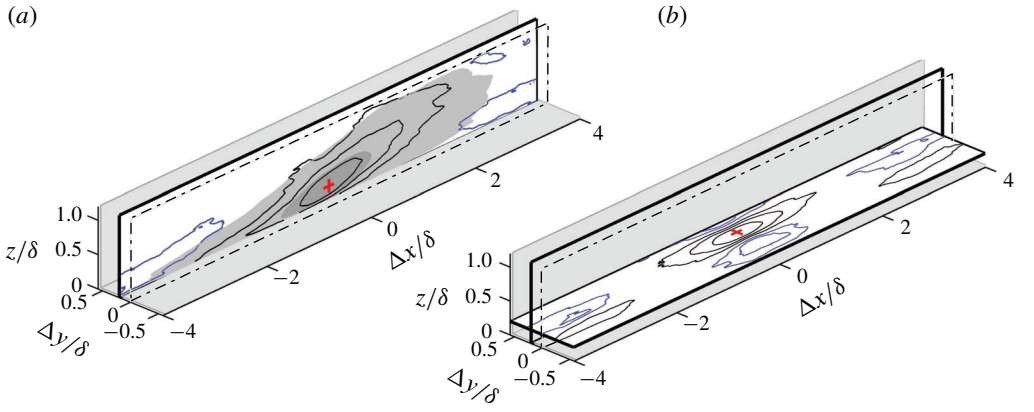

FIGURE 5. Maps of two-point correlation function $R_{u'u'}$ in the (*a*) *xz*- and (*b*) *xy*-planes about $(\Delta y_{ref}, z_{ref})/\delta = (0.2, 0.2)$. The + (red) symbols show the reference location. This reference position is also indicated in figure 4(*e*). Black contours lines: positive levels of 0.05, 0.15 and 0.3; blue contours lines: negative levels of −0.05 and −0.1. Grey contours on (*a*) show the contours of standard (streamwise- and spanwise-ensembled) two-point correlation with contour levels of 0.05 and 0.3. Dot-dashed planes indicate the middle of the domain, $\Delta y = 0$ plane.

the possible streamwise-repeating behaviour from the canonical smooth-wall flows. We first compute the correlation coefficient $R_{u'u'}$ at a spanwise position corresponding to the midpoint between the upwash- and downwash-flow regions. An analysis of figure 4(*e*) reveals that this point occurs at approximately $(\Delta y_{ref}, z_{ref})/\delta = (0.2, 0.2)$, as shown by the + (red) symbol in figure 4(*e*). The correlation $R_{u'u'}$ is calculated on the vertical and horizontal planes indicated by the solid lines in this figure. The reasoning behind selecting $\Delta y_{ref}/\delta = 0.2$ is that, at this spanwise location (i.e. the crossover between low-momentum/upwash and high-momentum/downwash regions), any meandering will lead to pronounced periodic fluctuations between positive and negative u'.

Figure 5(*a*) displays the resulting correlation map in the streamwise/vertical plane. The reference height $z_{ref}/\delta = 0.2$ corresponds to the centre of the mean roll-modes following Kevin *et al.* (2019), and we emphasise that changing the reference height within the outer layer has little effect on the present conclusions. Clearly the $R_{u'u'}$ map constructed in this manner differs substantially from the standard correlation map at the same reference height z_{ref}/δ (shown by grey filled contours in figure 5*a*), particularly for the larger-size coherence. When ensembled in this way, at a certain distance to the span of a detected large-scale event, a clear streamwise-repeating behaviour of positive and negative correlations manifests which would ordinarily be masked by the spanwise-averaging process of a standard two-point correlation. Note that when the correlation is computed about the upwash- and downwash-flow region, i.e. $y/\delta = 0$ and 0.45 in figure 4(*e*), the repeating pattern is not evident (not shown here for brevity). Figure 5(*b*) displays this alternating coherence in the wall-parallel slice, where again we see strong signs of streamwise periodicity (with streamwise alternating regions of positive and negative correlation) and a close resemblance to the behaviour observed in spanwise-heterogeneous boundary layers (Kevin *et al.* 2019).

Various interpretations can be drawn when observing an alternating sign of statistical pattern such as those shown in figure 5. Elsinga *et al.* (2010) proposed the

idea of larger vortex organisation where large-scale (mostly symmetrical) hairpin structures are arranged in an alternating configuration. However, as established previously, the outer-layer behaviour observed here is characterised by events with a much longer streamwise extent than would be implied from this interpretation. The more likely explanation based on the observations of figures 1 and 2, is simply that this periodicity is a result of meandering. This observation was concluded in spanwise-heterogeneous flows by Kevin *et al.* (2019) using a conditional analysis, where the meandering bend/turn is shown to be associated with a non-symmetrical wall-normal vortex structure.

4. A closer look at the representative streamwise roll-modes

In the conditionally averaged view, a pair of counter-rotating streamwise vortices, as represented in figure 4(*e*), are known to flank the large-scale turbulence structures (Hutchins, Hambleton & Marusic 2005; del Álamo *et al.* 2006; Dennis & Nickels 2011). In spanwise-heterogeneous wall flows, where the high- and low-momentum regions are spatially locked at fixed locations in the spanwise direction, these flanking vortices are readily apparent in the unconditional mean statistics as the counter-rotating 'secondary flows/roll-modes'. Instantaneously, however, Kevin *et al.* (2017) found that these secondary roll-modes are more often constituted by one-sided streamwise vortices than two-sided/counter-rotating motions. Hence, they concluded that turbulent secondary flows, whose time-averaged magnitude is often weak, are an artefact arising from superposition of the more typical non-symmetrical vortices within the spanwise-heterogeneous boundary layers.

In this section, by employing a similar sorting technique to Kevin *et al.* (2017), though this time applied to a smooth-wall (spanwise-homogeneous) boundary layer dataset, we aim to assess the likelihood of instantaneous streamwise vortices appearing symmetrically or otherwise. The sorting method is based on the instantaneous vertical velocity at three spanwise locations about the centre of the identified low-speed streak as illustrated in figure 6(*a*). The instantaneous w_f field is locally averaged within a spanwise width of 0.1δ (within the hatched region on figure 6*a*) to determine the main vertical-flow direction in these three detection locations. Note that these locations correspond to the upwash and downwash regions shown in figure 4(*e*). As an example, the combination result illustrated in figure 6(*a*) is 'negative–positive–negative' or $(-, +, -)$, which corresponds to a 'down–up–down' flow pattern. Thus, this particular instance represents a counter-rotating direction similar to figure 4(*e*). Note that there will be 2^3 sign/pattern combinations. We can then sort all the cross-stream (yz) slices along the detected structures identified in § 3.1, based on each combination. Accordingly, a conditionally averaged flow field can be produced for each pattern. If all combinations are included, we recover the generally accepted conditionally averaged vortices shown in figure 4(*e*).

Figure 6(*b*) displays the conditionally averaged field when the combination is $-, +, -$. As expected, counter-rotating vortices appear, resembling the typical quasi-streamwise counter-rotating rollers that on average border the turbulent events. Surprisingly, this pattern accounts for only 15 % of the instantaneous fields, while the large one-sided patterns, shown in figure 6(*c*,*d*), represent 32 %. Moreover, figure 6(*e*), which includes the other five combinations (i.e. $+, +, +$; $-, -, -$; $-, +, -$; $-, +, +$; $+, +, -$), where the individual result does not resemble the overall mean roll-modes, occupy the majority of the flow fields.

Although the exact fractions of each combination differs from the heterogeneous flow (Kevin *et al.* 2017), the key observations are consistent. Large streamwise

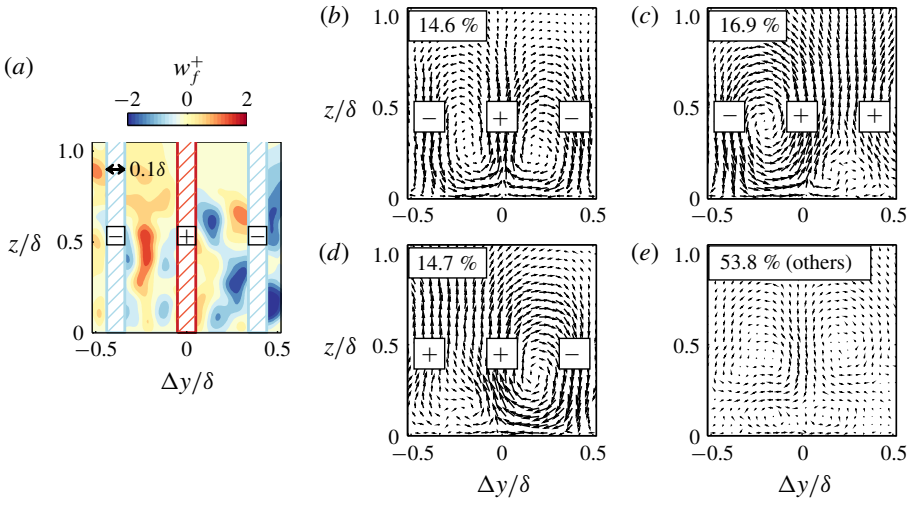

FIGURE 6. (*a*) An example of filtered wall-normal velocity field associated with large-scale low-momentum region. The hatched regions show the areas where w_f is averaged to determine the common vertical-flow directions. (*b*) Conditionally averaged vectors when the averaged-w_f is $-, +, -$. (*c*,*d*) Conditional vectors when the averaged-w_f is $-, +, +$ and $+, +, -$. (*e*) Conditional vectors for the remaining combinations. Vector size is comparable between figures.

rollers related to the turbulence structures are predominantly one-sided and rarely resemble the counter-rotating view. Hence, the representative eddy (and its weakness in strength, see figure 4*e*), are likely to be an artefact of the superposition of various turbulent events. Though statistically sound, the risk with allowing symmetrical representative eddies to dominate our interpretations (i.e packet models and attached eddy hypothesis) is that important dynamical processes can be obscured. For example, the meandering of the low-speed streaks and the one-side vortex structure is reminiscent of the streak-vortex model, as put forward by Jeong *et al.* (1997) in the near-wall region, and more recently described by Flores & Jiménez (2010) in the log layer. Certainly the current results indicate that the large-scale vortices occur intermittently in space, as suggested by the large number of instances along the structures, yielding a negligible contribution to the overall ensemble. These observations further support the conclusion of Lozano-Durán & Jiménez (2012), where they stated that the spanwise arrangements of large high- and low-speed events, which are directly related to the vortical structure between them, are more likely to occur as pairs (hence yield one-sided rotational motion) instead of in symmetric trios. Lastly, we note that the percentages shown in figure 6 resemble the meandering probability inferred by Hutchins *et al.* (2011), although their technique was limited to aggregating the contributions displayed here by figure 6(*b*,*e*) as the 'non-meandering events'.

5. Summary and schematic interpretation

Inspired by our previous findings in spanwise-heterogeneous boundary layers (Kevin *et al.* 2017, 2019), here we underline the pronounced unsteady behaviour of large-scale structures in canonical boundary layers. The relevant discussions are summarised below:

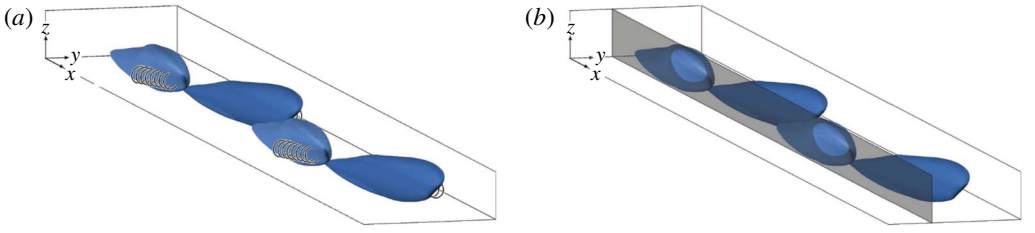

FIGURE 7. Conceptual three-dimensional interpretation of the shape and alignment of large low-momentum regions (blue iso-surface). (*a*) Illustration of the alternating one-sided streamwise vortices that flank these structures, and (*b*) the streamwise periodicity that occurs in the outer layer to the side of the large-scale structures. The shaded plane in (*b*) is approximately 0.2δ to the side of the centreline of the structures.

(i) The wall-parallel signature of large-scale structures becomes significantly meandering away from the wall. This trend is quantified by the meandering amplitude of the spines of the structures at each wall location. At the edge of the boundary layer, the severely yawed turbulent regions give rise to the oblique/diagonal coherence in the spanwise velocity, which was previously documented by Sillero *et al.* (2014) and de Silva *et al.* (2018) in the turbulent-intermittent region. Specifically, the low-momentum regions (i.e. the induced negative u fluctuations) typically associated with the vortex groups, are now resolved in the spanwise direction as v-velocities, giving them apparent diagonal coherence, as these large structures are increasingly tilted with wall height.

(ii) We unmask the dominant streamwise-repeating behaviour of the large-scale structures, which is always absent in the conventional average representation. We surmise that this behaviour is hidden in the typical spatial statistics due to spanwise averaging. This periodicity was previously observed by Kevin *et al.* (2019) in a spanwise-heterogeneous flow, where it was shown to signify the meandering wavelength of the turbulent structure.

(iii) Using a conditional sorting technique, we show that large quasi-streamwise vortices that exist alongside the low-momentum structures are predominantly one-sided. Additionally, we show that these accompanying vortex motions are highly intermittent spatially, and that for half the time the cross-stream signatures along low-momentum streaks do not contribute to the overall/representative (counter-rotating) vortex structure. It is restated that caution should be applied when portraying/reconstructing instantaneous flow fields using a representative structure with enforced symmetry, since it may obscure certain attributes which are of dynamical significance to the instantaneous turbulence structure.

Finally, we distil the above findings to create a conceptual representation of large-scale turbulence structure. The schematic drawing shown in figure 7 illustrates a 'train' of low-momentum regions. The appearance of each blue region adheres to the widely accepted representative/average shape, i.e. streamwise-elongated coherence with a shallow forward inclination angle. However, here we portray the structure to be slightly tilted from the vertical axis. As indicated here by figure 6 and by Kevin *et al.* (2017), this behaviour implies that non-symmetrical/one-sided streamwise vortex structures are dominant, and are formed underneath the leaning eruption of the low-momentum structure. Furthermore, if we take a streamwise/vertical slice at a spanwise location sideways from the spanwise centre of this train of structures, such

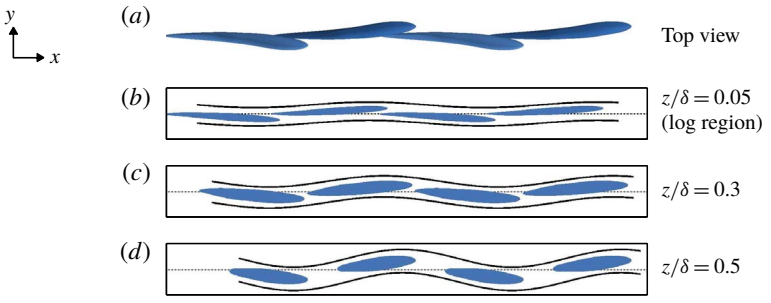

FIGURE 8. (*a*) Top view of the model. (*b–d*) Streamwise/spanwise wall-parallel slices.

as illustrated in figure 7(*b*), a repeating pattern will be evident in the outer layer. Figure 8(*a*) further displays the top view of this illustrative model. The importance here is that, when this train of structures is sliced horizontally in the log region, the velocity signature exhibits a weakly meandering behaviour. In the outer layer, however, this configuration will produce a wider signature with a stronger meandering tendency and a steeper tilting angle.

We note that these δ-scale behaviours closely resemble the buffer-layer model of Jeong *et al.* (1997), Schoppa & Hussain (2002), and their temporal evolution can perhaps be inferred from the 'minimal flow' study shown in figure 24(c) in the review by Jiménez (2018). Overall, these similarities suggest that small- and large-scale coherence may exhibit similar unstable dynamical behaviour (Flores & Jiménez 2010; Hwang & Cossu 2010, 2011), and that a self-sustaining mechanism not dissimilar to that proposed for the near-wall region exists at a hierarchy of scales across turbulent boundary layers.

Acknowledgements

The authors thank the Australian Research Council for supporting this research. We also thank Professor J. Jiménez and Dr Y. S. Kwon for making the DNS datasets available, as well as to Dr C. de Silva for sharing the PIV data.

References

ADRIAN, R. J., CHRISTENSEN, K. T. & LIU, Z. C. 2000*a* Analysis and interpretation of instantaneous turbulent velocity fields. *Exp. Fluids* **29** (3), 275–290.

ADRIAN, R. J., MEINHART, C. D. & TOMKINS, C. D. 2000*b* Vortex organization in the outer region of the turbulent boundary layer. *J. Fluid Mech.* **422**, 1–54.

DEL ÁLAMO, J. C., JIMÉNEZ, J., ZANDONADE, P. & MOSER, R. D. 2006 Self-similar vortex clusters in the turbulent logarithmic region. *J. Fluid Mech.* **561**, 329–358.

BAI, H. L., KEVIN, K., HUTCHINS, N. & MONTY, J. P. 2018 Turbulence modifications in a turbulent boundary layer over a rough wall with spanwise-alternating roughness strips. *Phys. Fluids* **30** (5), 055105.

BAIDYA, R., DE SILVA, C. M., HUANG, Y., CASTILLO, L., MARUSIC, I. & HUTCHINS, N. 2016 Developing turbulent boundary layer using spanwise-periodic trips. In *20th Australasian Fluid Mechanics Conference, Perth, Australia*.

DENNIS, D. J. C. & NICKELS, T. B. 2011 Experimental measurement of large-scale three-dimensional structures in a turbulent boundary layer. Part 1. Vortex packets. *J. Fluid Mech.* **673**, 180–217.

ELSINGA, G. E., ADRIAN, R. J., VAN OUDHEUSDEN, B. W. & SCARANO, F. 2010 Three-dimensional vortex organization in a high-Reynolds-number supersonic turbulent boundary layer. *J. Fluid Mech.* **644**, 35–60.

FLORES, O. & JIMÉNEZ, J. 2010 Hierarchy of minimal flow units in the logarithmic layer. *Phys. Fluids* **22** (7), 071704.

GANAPATHISUBRAMANI, B., HUTCHINS, N., HAMBLETON, W. T., LONGMIRE, E. K. & MARUSIC, I. 2005 Investigation of large-scale coherence in a turbulent boundary layer using two-point correlations. *J. Fluid Mech.* **524**, 57–80.

HUTCHINS, N., CHAUHAN, K., MARUSIC, I., MONTY, J. & KLEWICKI, J. 2012 Towards reconciling the large-scale structure of turbulent boundary layers in the atmosphere and laboratory. *Boundary-Layer Meteorol.* **145** (2), 273–306.

HUTCHINS, N., HAMBLETON, W. T. & MARUSIC, I. 2005 Inclined cross-stream stereo particle image velocimetry measurements in turbulent boundary layers. *J. Fluid Mech.* **541**, 21–54.

HUTCHINS, N. & MARUSIC, I. 2007 Evidence of very long meandering features in the logarithmic region of turbulent boundary layers. *J. Fluid Mech.* **579**, 1–28.

HUTCHINS, N., MONTY, J. P., GANAPATHISUBRAMANI, B., NG, H. C. H. & MARUSIC, I. 2011 Three-dimensional conditional structure of a high-Reynolds-number turbulent boundary layer. *J. Fluid Mech.* **673**, 255–285.

HWANG, Y. & COSSU, C. 2010 Self-sustained processed at large scales in turbulent channel flow. *Phys. Rev. Lett.* **105** (4), 044505.

HWANG, Y. & COSSU, C. 2011 Self-sustained processes in the logarithmic layer of turbulent channel flows. *Phys. Fluids* **23** (6), 061702.

JEONG, J., HUSSAIN, F., SCHOPPA, W. & KIM, J. 1997 Coherent structures near the wall in a turbulent channel flow. *J. Fluid Mech.* **332**, 185–214.

JIMÉNEZ, J. 2018 Coherent structures in wall-bounded turbulence. *J. Fluid Mech.* **842**, P1.

JIMÉNEZ, J. & SIMENS, M. P. 2001 Low-dimensional dynamics of a turbulent wall flow. *J. Fluid Mech.* **435**, 81–91.

JOHANSSON, A. V., ALFREDSSON, P. H. & KIM, J. 1991 Evolution and dynamics of shear-layer structures in near-wall turbulence. *J. Fluid Mech.* **224**, 579–599.

KEVIN, MONTY, J. P., BAI, H. L., PATHIKONDA, G., NUGROHO, B., BARROS, J. M., CHRISTENSEN, K. T. & HUTCHINS, N. 2017 Cross-stream stereoscopic particle image velocimetry of a modified turbulent boundary layer over directional surface pattern. *J. Fluid Mech.* **813**, 412–435.

KEVIN, MONTY, J. P. & HUTCHINS, N. 2019 Turbulent structures in a statistically three-dimensional boundary layer. *J. Fluid Mech.* **859**, 543–565.

LEE, J., LEE, J. H., CHOI, J. I. & SUNG, H. J. 2014 Spatial organization of large- and very-large-scale motions in a turbulent channel flow. *J. Fluid Mech.* **749**, 818–840.

LEE, J. H. & SUNG, H. J. 2011 Very-large-scale motions in a turbulent boundary layer. *J. Fluid Mech.* **673**, 80–120.

LOZANO-DURÁN, A. & JIMÉNEZ, J. 2012 The three-dimensional structure of momentum transfer in turbulent channels. *J. Fluid Mech.* **694**, 100–130.

MARUSIC, I. & MONTY, J. P. 2019 Attached eddy model of wall turbulence. *Annu. Rev. Fluid Mech.* **51**, 49–74.

MONTY, J. P., STEWART, J. A., WILLIAMS, R. C. & CHONG, M. S. 2007 Large-scale features in turbulent pipe and channel flows. *J. Fluid Mech.* **589**, 147–156.

SCHOPPA, W. & HUSSAIN, F. 2002 Coherent structure generation in near-wall turbulence. *J. Fluid Mech.* **453**, 57–108.

SILLERO, J. A., JIMÉNEZ, J. & MOSER, R. D. 2014 Two-point statistics for turbulent boundary layers and channels at Reynolds numbers up to $\delta^+ \approx 2000$. *Phys. Fluids* **26** (10), 105109.

DE SILVA, C. M., KEVIN, BAIDYA, R., HUTCHINS, N. & MARUSIC, I. 2018 Large coherence of spanwise velocity in turbulent boundary layers. *J. Fluid Mech.* **847**, 161–185.

TOMKINS, C. D. & ADRIAN, R. J. 2003 Spanwise structure and scale growth in turbulent boundary layers. *J. Fluid Mech.* **490**, 37–74.

VANDERWEL, C. & GANAPATHISUBRAMANI, B. 2015 Effects of spanwise spacing on large-scale secondary flows in rough-wall turbulent boundary layers. *J. Fluid Mech.* **774**, R2.